NASA Technical Memorandum 105311

A Study of $Na_xPt_3O_4$ as an O_2 Electrode Bifunctional Electrocatalyst

William L. Fielder and Joseph Singer
Lewis Research Center
Cleveland, Ohio

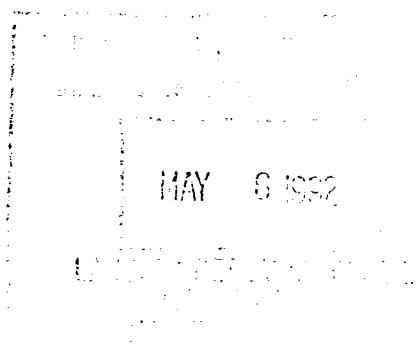

December 1991

NASA

A STUDY OF $Na_XPt_3O_4$ AS AN O_2 ELECTRODE BIFUNCTIONAL ELECTROCATALYST

W.L. Fielder and J. Singer
National Aeronautics and Space Administration
Lewis Research Center
Cleveland, Ohio 44135

SUMMARY

The present study suggests that PTFE-bonded $Na_XPt_3O_4$ gas porous diffusion electrodes may be a viable candidate for bifunctional O_2 reduction and evolution activity. The electrodes exhibited Tafel slopes of about 0.06 V/decade for both O_2 reduction and evolution. For O_2 reduction, the 0.06 slope doubled to 0.12 V/decade at larger current densities. Preliminary stability testing at 24 °C suggested that the $Na_XPt_3O_4$ electrodes were relatively stable at reducing and oxidizing potentials typically encountered at the O_2 electrode in a regenerative fuel cell.

INTRODUCTION

Efficient, long-life energy storage systems will be required for many future NASA missions such as LEO or GEO space platforms and lunar or martian bases. One candidate for these missions is the alkaline regenerative H_2-O_2 fuel cell in conjunction with a photovoltaic array. For example, the dedicated two-unit H_2-O_2 system consists of a fuel cell which uses H_2 and O_2 to produce power during the dark portion and of an electrolyzer which uses power to regenerate the H_2 and O_2 during the light portion.

Some of the more desirable characteristics for H_2-O_2 fuel cell systems, particularly for long-time automated operation, are high energy density, small volume, high efficiency, high reliability and long life. A recent GEO mission analysis indicated that a significant increase in energy density is possible if a two-unit alkaline fuel cell and electrolyzer system is replaced with a single-unit alkaline fuel cell/electrolyzer system (ref. 1).

The efficiencies of fuel cell and electrolyzer systems under load are considerably less than 100 percent due, primarily, to the irreversibility of the O_2 electrode. Therefore, active bifunctional O_2 electrocatalysts are needed to increase the kinetics for both O_2 reduction and evolution to maximize the efficiency of a single-unit alkaline fuel cell/electrolyzer system.

Metals and oxides have been investigated as candidates for monofunctional O_2 electrocatalysts for alkaline fuel cells and electrolyzers. For example, a Au-10 percent Pt electrocatalyst, developed by International Fuel Cells Corporation (IFC), is being used as a cathode for O_2 reduction in the space shuttle's alkaline H_2-O_2 fuel cell (refs. 2 and 3). Similarly, $NiCo_2O_4$ may be an attractive electrocatalyst candidate for O_2 evolution in an alkaline electrolysis cell (refs. 4 and 5). Studies of bifunctional O_2 electrocatalysts, however, are rare or unpublished.

In addition to showing acceptable bifunctional O_2 activity, a long-life candidate must also be stable under both reducing and oxidizing conditions. Although Pt and Pt alloys exhibit moderate bifunctional O_2 electrode activity, long-time stability for Pt, particularly during O_2 evolution, is questionable. Pt bronzes, composed of oxides of Pt and an alkali metal, are

believed to have greater stability than metallic Pt particularly under oxidizing potentials. Na-Pt bronze powders (i.e., $Na_XPt_3O_4$) have been prepared by Giner, Inc. as single phase and in moderately high surface area. Giner, Inc. fabricated PTFE-bonded gas porous diffusion electrodes for the present study using mixtures of $Na_XPt_3O_4$ powders as the electrocatalyst and polytetrafluoroethylene (PTFE) as the binder.

The objective of the present study is to ascertain the usefulness of $Na_XPt_3O_4$ as a bifunctional O_2 electrocatalyst for the O_2 electrode under alkaline conditions. Therefore, O_2 reduction and evolution activities and the stabilities of these PTFE-bonded electrodes were determined under both reducing and oxidizing conditions.

EXPERIMENTAL

$Na_XPt_3O_4$ Preparation and Electrode Fabrication

Giner, Inc. prepared two similar batches (A and B) of single phase $Na_XPt_3O_4$ powder by heating pellets of Na_2CO_3 and $PtO_2 \cdot H_2O$ to about 650 °C under an atmosphere of O_2 (refs. 6 and 7). The Na content in the $Na_XPt_3O_4$ powder was estimated from the lattice constant a_o obtained by x-ray diffraction. The relationship is as follows:

$$a_o = 0.11X + 5.585 \quad (1)$$

where X represents the Na content (ref. 8). Lattice constants of 5.673 and 5.668 Å were obtained for batches A and B, respectively. Therefore, compositions of about $Na_{0.80}Pt_3O_4$ and $Na_{0.75}Pt_3O_4$ were calculated for the two batches from equation 1. X-ray diffraction analysis showed no free Pt in either batch. The BET surface area was about 17 m^2/g for both batches. The conductivity of a compacted pellet of this $Na_XPt_3O_4$ powder, determined by a 2-probe resistance measurement, was about 50 Ω-cm^{-1}.

Giner, Inc. fabricated 4 PTFE-bonded gas porous diffusion electrodes using batch A powder for electrodes 1 and 2 and batch B powder for electrodes 3 and 4. The PTFE contents for these 4 electrodes ranged between 20 and 35 percent of the $Na_XPt_3O_4$. For each electrode, the catalyst-PTFE mixture was pressed with a Au plated Ni screen current collector and a Gortex[1] porous PTFE backing to form a "green" electrode. The Gortex backing serves as a barrier to the KOH electrolyte at the gas side but not to gaseous O_2. The resulting "green" electrodes was then heated at about 350 °C, by means of a proprietary procedure, to form the PTFE-bonded gas porous diffusion electrode. The loadings and PTFE contents for electrodes 1, 2, 3 and 4 are listed in table I.

O_2 reduction measurements for electrodes 1, 2, 3 and 4 indicated that O_2 transport became rate-controlling at relatively small current densities. Therefore, Giner, Inc. fabricated electrode 5 with a more balanced hydrophobic and hydrophilic catalyst-PTFE mix using $Na_{0.75}Pt_3O_4$ powder (batch B) in an attempt to increase the O_2 transport during O_2 reduction. The loading and PTFE content for electrode 5 are also listed in table I.

---

[1]Gortex is a trade name of W.L. Gore & Co.

Electrochemical Apparatus and Measurements

A floating electrode half-cell apparatus was used for all electrochemical measurements (ref. 9). A schematic of the floating half-cell is shown in figure 1. The PTFE-bonded electrode served as the working electrode with Au wire serving as the counter electrode. The reference electrode was a Hg/HgO electrode with a potential of 0.926 V versus a reversible H_2 electrode (RHE) in the same solution at 25 °C.[2] The temperature coefficient for this reference electrode is about -0.45 mV/°C as determined by comparison with a dynamic H_2 electrode at various temperatures (fig. 2). An atmosphere of gaseous O_2 (N_2) was passed through a presaturator to minimize H_2O loss in the half-cell.

Current-potential data were obtained galvanostatically by means of manual or computer driven systems. Both methods gave essentially the same values. For the computer driven system, the potentiostat (EG&G Princeton Applied Research Model 173) was interfaced with an Apple IIe computer by means of a EG&G Model 276 plug-in unit. A computer program (EG&G Electrochemistry Program Volume I) was used to drive and control the potentiostat.

iR polarizations were determined by means of an Electrosynthesis Corp. Model 800 IR instrument in conjunction with a 7 V Zener diode. The instrument interrupts the circuit periodically for a few microseconds. The diode limits the voltage rise to 7 V during the interruption. iR polarization values for correcting observed potentials were obtained from a plot of iR against current as illustrated in figure 3 for a typical run.

Experimental Procedure

The working electrode was introduced into the floating electrode half-cell to obtain the current-potential data with the electrocatalyst side of the electrode contacting the surface of the 30 percent KOH electrolyte. The electrode was then raised slightly to form a small meniscus at the electrode/electrolyte interface. Exact positioning of the electrode was not critical for determining the iR corrected potentials for small meniscus heights. For example, while an observed potential and iR may vary slightly with electrode positioning, the corresponding iR corrected potential remained essentially constant for a fixed current.

PTFE-bonded electrodes, operating as cathodes in an alkaline electrolyte, generally benefit from cathodic preconditioning to minimize initial polarization. Therefore, each electrode was preconditioned by slowly increasing the cathodic current to greater than -0.8 A while maintaining the potential above 0.3 V. This preconditioning process may require up to 0.5 hr.

Steady-state current-potential data were then obtained galvanostatically starting at the larger cathodic or anodic currents. At larger anodic currents, the potentials (and iR values) became erratic as illustrated in figure 4. Rapid O_2 evolution may force some of the KOH electrolyte out of the smaller pores (ref. 10). In addition, detachment of the O_2 bubbles, formed at the electrode/electrolyte interface, may become increasingly more difficult, particularly if these bubbles become trapped inside the tube holding the electrode. Therefore, O_2 evolution data were not recorded for anodic currents larger than 0.2 to 0.4 A/cm^2. For moderate currents, a steady-state condition was usually obtained after a relatively short time. Smaller currents may

[2]All potential values in this report will refer to RHE unless otherwise stated.

require slightly longer times. As an illustration, a steady-state condition was obtained after about 10 sec for an anodic run at 0.05 A/cm^2 while about 180 sec were required at 0.001 A/cm^2.

Preliminary runs had indicated that a working electrode may undergo a small irreversible change during cathodic aging even though it had been preconditioned previously. This is illustrated in figure 5 where the potential for the preconditioned electrode 5 increased slowly during the first 30 min. After this initial aging period, the potential remained essentially constant with time. Therefore, all electrodes were aged cathodically at about -0.01 A/cm^2 (or anodically at about 0.01 A/cm^2) for about 4 hr prior to obtaining the respective O_2 reduction or evolution data. Current-potential data were then obtained galvanostatically.

The stabilities of electrode 5 at 24 °C were followed, both in the presence of O_2 and under an inert atmosphere of N_2, for longer periods.

For stability determinations under an inert atmosphere, electrode 5 was introduced into the half-cell under flowing N_2 and submerged below the surface of the KOH. For the first series of tests, corrosion currents were obtained. A cyclic voltammogram at 1 mV/sec over a large potential range gave very broad oxidation-reduction peaks at about 0.9 and 0.7 V as shown in figure 6. Therefore, a potential of 0.6 V was chosen for the corrosion measurements. The electrode was held potentiostatically at 0.6 V for 7 hr and the resulting cathodic currents were recorded periodically. For the second series of tests under N_2, electrode capacitances at about 0.45 V were calculated for a submerged electrode. The cyclic voltammogram in figure 6 had indicated that oxidation-reduction reactions are minimal between about 0.4 and 0.5 V. An initial cyclic voltammogram was obtained between 0.4 and 0.5 V at 1 mV/sec (fig. 7(a)). After this initial cyclic sweep, the electrode was then held at 0.6 V for a total of about 305 hr. The run was interrupted periodically and the cyclic sweeps were repeated to redetermine the electrode capacitances. The cyclic voltammogram at the end of the 305 hr is shown in figure 7(b).

For stability determinations in the presence of O_2, electrode 5 was placed in the floating half-cell in a manner similar to that used to obtain the current-potential data. For the first series of tests, the electrode was held anodically at 0.01 A for 121 hr. At the end of this period, the current was reversed and the sample was held cathodically at -0.01 A for 100 hr and then at -0.1 A for an additional 60 hr. For the second series of tests under O_2, another sample of electrode 5 was cycled at alternate periods of about 24 hr at anodic and cathodic currents of 0.01 and -0.01 A/cm^2. The potentials were recorded periodically during the 340 hr run. For a third series of tests, another sample of electrode 5 was cycled continuously under both reducing and oxidizing conditions. Initially, the electrode was held at 0.827 V for 60 sec and the initial cathodic current was recorded. Then, the electrode was swept continuously at 1 mV/sec between 0.827 and 1.446 V. The cycling was interrupted periodically and the cathodic currents were redetermined at 0.827 V. This procedure was repeated for a total of 1132 cycles (390 hr).

RESULTS AND DISCUSSION

O_2 Reduction

The Na content in electrode 1 and 2 differed somewhat from that in electrodes 3 and 4 with compositions of about $Na_{0.80}Pt_3O_4$ and $Na_{0.75}Pt_3O_4$, respectively. It is assumed, however,

that this small change in Na composition is not a major factor in controlling the kinetics of O_2 reduction.

Current-potential O_2 reduction data were obtained for aged electrodes 1, 2, 3 and 4 at 80 °C. Polarization potentials were calculated by subtracting the iR corrected potentials from the corresponding thermodynamic potential (i.e., 1.181 V at 80 °C). Tafel plots were obtained by plotting these polarization potentials against the logarithms of the geometric current densities. The Tafel data for each of these 4 electrodes could be fitted to two straight line regions. This is illustrated in figure 8 for electrode 3 where the O_2 reduction data at 80 °C were fitted to 2 regions with slopes of about 0.06 and 0.12 V/decade. The corresponding intercepts for these 4 electrodes are listed in table II.

The $Na_XPt_3O_4$ loading levels for electrodes 1, 2, 3 and 4 varied between 13.6 and 24.5 mg/cm^2 of geometric area (table I). It seems reasonable to assume that the kinetics for O_2 reduction can be normalized to the $Na_XPt_3O_4$ loading levels if the electrode structures are similar. Therefore, the geometric exchange current densities for O_2 reduction for these 4 electrodes were normalized to 20 mg/cm^2 of $Na_XPt_3O_4$ at 80 °C. These values are also listed in table II. O_2 reduction Tafel data were calculated for the 4 electrodes using the normalized geometric exchange current densities and the slopes. The resulting plots are shown in figure 9.

One model for PTFE-bonded gas porous diffusion electrodes assumes that catalyst particles form porous electrode agglomerates which are flooded with electrolyte and that the PTFE creates hydrophobic gas channels. When current is drawn from the electrode, the gas diffuses through the hydrophobic channels, dissolves in the electrolyte in the agglomerate and then reacts at the catalyst surface sites (ref. 11). A mathematical model for this type of electrode suggested that at smaller or moderate current densities, where the catalyst is utilized more effectively, the reaction process is activation controlled with a Tafel slope value that is essentially equal to that of a smooth electrode. However, at larger current densities, where the catalyst is not so well utilized, the reaction process changes from activation control to diffusion control with a corresponding Tafel slope of about double that for a smooth electrode (ref. 12).

The Tafel slope for O_2 reduction at electrodes 1, 2, 3 and 4 increased from 0.06 to 0.12 V/decade. Similar to that suggested in reference 12, this doubling of the slope is believed to be indicative of a change from activation control for the 0.06 region to diffusion control for the 0.12 region. As seen in figure 9, this change to diffusion control occurred at relatively small current densities. This suggests that electrodes 1, 2, 3 and 4 were too hydrophobic leading to insufficient KOH access. Improved O_2 reduction performance may require a better balance between the hydrophobic and hydrophilic electrode character.

Even though all 4 electrodes were assumed to be excessively hydrophobic, figure 9 suggests that the PTFE content is still an important factor to be considered for improving the O_2 reduction performance at $Na_XPt_3O_4$ electrodes. This is illustrated by the O_2 reduction activity for the 4 electrodes which increased with increasing PTFE content. For example, the polarizations for electrodes 3 and 4, containing 30 and 35 percent PTFE, were considerably smaller than that obtained for electrode 1 (20 percent PTFE).

As will be discussed later, the reverse effect was observed for O_2 evolution. Smaller PTFE contents of 20 to 25 percent may lead to increased O_2 evolution activity. Optimization of a $Na_XPt_3O_4$ electrode for maximum bifunctional O_2 reduction and evolution activity may require an intermediate PTFE content in addition to a more balanced hydrophobic/hydrophilic

character. Therefore, Giner, Inc. fabricated electrode 5 with a PTFE content of 25 percent and a better balance in its wettability in an attempt to utilize a larger portion of the electrode interior and to increase the O_2 transport to this surface.

O_2 reduction data were then obtained for aged electrode 5 at temperatures ranging between 24 and 93 °C. The corresponding intercepts and geometric exchange current densities for electrode 5 are listed in table III. While only 2 regions were observed for electrodes 1, 2, 3 and 4 for the current density ranges used, data for electrode 5 could be fitted to 3 straight line regions for each temperature. This is illustrated in figure 10 where the data at 24 °C were fitted to lines with slopes of 0.04, 0.06, and 0.12 V/decade. Presumably, the 0.04 region would have been obtained for electrodes 1, 2, 3 and 4 if sufficiently small current densities had been used. Similar to the assumption made for electrodes 1, 2, 3 and 4, the observed doubling of the Tafel slope from 0.06 to 0.12 V/decade for electrode 5 suggests that diffusion is controlling for the 0.12 region.

The data for electrode 3 is also shown in figure 10 as a dashed line for comparison. This comparison indicates that utilization of the electrocatalyst in electrode 5 was greatly increased by the improved electrode structure and an increased wettability of this electrode. For example, the geometric exchange current density for electrode 5 at 80 °C for the 0.06 V/decade region is about 4.5×10^{-7} A/cm^2. The corresponding normalized geometric exchange current density for electrode 2 was about 2 orders of magnitude smaller. In addition, diffusion becomes rate controlling for electrode 5 at 80 °C at about 0.2 A/cm^2. The corresponding value for electrode 4 was a much smaller value (i.e., 0.004 A/cm^2).

The O_2 reduction data for electrode 5 for the various temperatures are shown in figure 11. The polarizations for O_2 reduction decreased with increasing temperatures indicative of an activation process.

The "apparent" energy of activation, E_A^*, for O_2 reduction at electrode 5 was calculated as follows:

$$E_a^* = -(2.3R)\left[\frac{d \log i_o}{d(1/T)}\right] \qquad (2)$$

where R is the gas constant and i_o is the exchange current density (ref. 13). A value of about 5.6 kcal/mol was calculated for the "apparent" energy of activation for O_2 reduction at electrode 5 for the 0.06 V/decade region (fig. 12(a)). An even smaller value of about 3.4 kcal/mol was calculated for the 0.12 region (fig. 12(b)). This smaller value for the 0.12 region (<5 kcal/mol) may be indicative of a largely diffusion controlled process (ref. 14 and 15). This is in agreement with the previous assumption that the doubling of the slope from 0.06 to 0.12 V/decade indicated a change from activation to diffusion control.

O_2 reduction data for electrode 5 at 80 °C are compared in figure 13 with data reported for a similar type of PTFE-bonded $Na_XPt_3O_4$ electrode at 80 °C (ref. 6) and with data reported for an IFC Orbiter Au-10 percent Pt fuel cell electrode (ref. 3). Giner, Inc. reported data for an electrode which used a loading of about 20 mg/cm^2 $Na_{0.8}Pt_3O_4$ powder (20 m^2/g) and a PTFE content of about 25 percent PTFE (ref. 6). Polarization values were estimated from the data

taken from the figure in reference 6 and these values are shown in figure 13 as triangles. The O_2 reduction polarization for the electrode reported in reference 6 was somewhat smaller than that which was obtained for electrode 5. This difference in polarization, however, was not large and may have been due to a more complete optimization of the reference 6 electrode. Data was reported for an IFC Orbiter fuel cell electrode (ref. 3). This electrode contained Au-10 percent Pt powder (10-15 m^2/g) as the electrocatalyst. These data are presented in figure 13 as a dotted line with slopes of about 0.04 and 0.12 V/decade. The polarization for the IFC electrode was somewhat smaller than that of electrode 5 and was essentially equal to that estimated from the figure in reference 6.

O_2 Evolution

Current-potential O_2 evolution data were obtained for aged electrodes 1, 2, 3 and 4 at 80 °C. The iR corrected Tafel data for electrodes 1, 3 and 4 could be fitted to 2 straight line regions. This is illustrated in figure 14 where the O_2 evolution data for electrode 1 were fitted to 2 regions with slopes of 0.06 and 0.12 V/decade. However, the data for electrode 2 could be fitted to three regions as shown in figure 15. In addition to the 0.06 and 0.12 regions, the data for electrode 2 were fitted to a line with a slope of 0.04 V/decade at the smaller current densities. Presumably, the 0.04 region would have also been observed for electrodes 1, 3 and 4 if sufficiently small current densities had been used. The corresponding intercepts for these 4 electrodes are listed in Table IV. The geometric exchange current densities for these 4 electrodes at 80 °C were normalized to 20 mg/cm^2 and these values are also listed in table IV. O_2 evolution Tafel data were calculated for these electrodes and the results are shown in figure 16.

Similar to that assumed for O_2 reduction, the doubling of the slope for the 0.06 and 0.12 V/decade region may be indicative of a change from activation to diffusion control. Even though all 4 of these electrodes were assumed to be excessively hydrophobic, figure 16 suggests that PTFE content is still one factor to be considered for improving the O_2 evolution performance at $Na_XPt_3O_4$ electrodes. For example, while the 0.12 region for electrode 4 started at about 0.001 A/cm^2, it started at about 0.01 A/cm^2 for electrodes 2 and 3. The data for electrode 5, however, as discussed below, suggested that a more balanced wettability of the electrode may be more important than PTFE content alone.

O_2 evolution data were then obtained for aged electrode 5 at temperatures between 24 and 88 °C. The data for each temperature could be fitted to one straight line region with a slope of about 0.06 V/decade. A slight deviation from the 0.06 region occurred at larger current densities for each temperature as illustrated in figure 17 for data obtained at 88 °C. It is assumed that this small deviation was due to the formation of O_2 bubbles at the bottom of the electrode which became trapped inside the half-cell tube holding the electrode. The corresponding intercepts and geometric exchange current densities are listed in Table V. The doubling of the Tafel slope from 0.06 to 0.12 V/decade region was not observed for electrode 5 at larger current densities since O_2 bubble formation and mass transfer polarization limited measurements to currents of about 0.1 to 0.2 A/cm^2.

The O_2 evolution data for electrode 5 data for the various temperatures are shown in figure 18. The polarizations for O_2 evolution decreased with increasing temperatures indicative of an activation process. The geometric exchange current densities for O_2 evolution for electrode 5 were calculated and the corresponding logarithms were plotted in figure 19 against the reciprocals of the absolute temperatures. The "apparent" energy of activation for O_2 evolution for this region is about 9.5 kcal/mol.

O_2 evolution data for electrode 5 at 88 °C are compared in figure 20 with data reported for a similar type of PTFE-bonded $Na_XPt_3O_4$ electrode at 80 °C (ref. 6) and with data reported for an active $NiCo_2O_4$ electrode (ref. 5). Polarization values were estimated from data taken from the figure in reference 6 and these values are shown in figure 20 as triangles. The polarization for the reference 6 electrode was essentially equal to that obtained for electrode 5 for the 0.06 region. The polarization values for the $NiCo_2O_4$ electrode are presented in figure 20 as a dotted line with slopes of 0.06 and 0.12 V/decade. The polarization for the $NiCo_2O_4$ electrode is essentially equal to that of electrode 5 for the 0.06 region.

Voltage Efficiency

Although O_2 reduction and evolution reactions at $Na_XPt_3O_4$ are not reversible as illustrated in figure 21 for electrode 5, the PTFE-bonded gas porous diffusion $Na_XPt_3O_4$ electrode appears to be a viable candidate for a bifunctional O_2 electrode for a single-unit, alkaline H_2-O_2 fuel cell/electrolyzer system

Although these $Na_XPt_3O_4$ electrodes have not yet been fully optimized for maximum bifunctional O_2 activity, it is of interest to estimate voltage efficiencies for assumed fuel cell/electrolyzer operating conditions using $Na_{0.75}Pt_3O_4$ electrode 5 as the bifunctional O_2 electrode. The iR corrected voltage efficiency, V_e, for the O_2 electrode may be defined as follows:

$$V_e = \left(\frac{E_R}{E_O}\right) \times 100 \tag{3}$$

where E_R is the reduction potential produced during the fuel cell operation and E_O is the oxidation potential required during the electrolyzer operation. Voltage efficiencies for O_2 reduction-oxidation reactions at electrode 5 may be estimated using the activation energy plots. As an illustration, geometric exchange current densities for O_2 reduction and evolution were estimated for an assumed operation at 100 °C and at geometric current densities of -0.1 A/cm^2 and 0.1 A/cm^2. These operating conditions were selected for the illustration since they represent modest goals for a single-unit fuel cell/electrolyzer system. For the case of O_2 reduction, extrapolation of the data for the 0.06 V/decade region to 100 °C (Fig. 12(a)) gives a geometric exchange current density of about 6.4×10^{-7} A/cm^2. An O_2 electrode potential of about 0.847 V is calculated for -0.1 A/cm^2. A corresponding potential of about 1.377 V is calculated for O_2 evolution at 0.1 A/cm^2. Therefore, a value of about 60 percent is estimated for the voltage efficiency (iR corrected) for 100 °C and 0.1 A/cm^2. For comparison, a value of about 55 percent is calculated for 25 °C and 0.1 A/cm^2.

$Na_XPt_3O_4$ Electrode Stability

The stability of electrode 5 ($Na_{0.75}Pt_3O_4$) was examined at 24 °C in the presence of both N_2 and O_2. Testing under an inert atmosphere of N_2 may allow changes in the composition of $Na_{0.75}Pt_3O_4$ to be seen more easily. For example, $Na_{0.75}Pt_3O_4$ in the presence of O_2 is an active electrocatalyst for O_2 reduction and may mask smaller cathodic currents produced by reduction of $Na_{0.75}Pt_3O_4$. For the first series of tests under N_2, a submerged sample of electrode 5 was held at 0.6 V for 7 hr at 24 °C. Cathodic currents were recorded periodically. These currents,

normalized to 1 mg of $Na_{0.75}Pt_3O_4$, are plotted in figure 22 against the reciprocals of the square root of time. Extrapolation to infinite time yields a value of less than 0.1 μA/mg of $Na_{0.75}Pt_3O_4$. A very small cathodic current is not an absolute indicator of the electrocatalyst's stability to electrochemical reduction. Other factors, such as delamination of the electrocatalyst from the current collector, may also lead to deceptively small currents. However, no visible changes or delamination were observed for electrode 5 after the run. Therefore, this extremely small cathodic current is assumed to represent reduction processes. The following processes may have contributed to the production of these small currents: reduction of $Na_{0.75}Pt_3O_4$; reduction of trace quantities of O_2 in the N_2 atmosphere; and reduction of trace impurities present in the KOH electrolyte. For example, currents of the order of 0.01 to 0.1 μA/mg have been observed for a Au screen current collector under similar conditions. These currents (using the Au screen) were due, presumably, to reduction of trace quantities of O_2 in the N_2 atmosphere. Therefore, it seems reasonable to assume that the cathodic current of less than 0.1 μA/mg (Fig. 22), is an upper limit for the corrosion current of $Na_{0.75}Pt_3O_4$. If this be the case, this relatively small value suggests relatively good stability for $Na_{0.75}Pt_3O_4$ under reducing potentials.

A second series of stability tests under flowing N_2 involved holding a sample of electrode 5 at 0.6 V for 305 hr at 24 °C with periodic interruptions for obtaining cyclic voltammograms. If electrode capacitances are obtained at potentials where reduction processes are minimal, the results may indicate whether changes in electrode surface area are occurring during the 0.6 V run. As shown in figure 7(a), the current for electrode 5 rose rapidly during the charging of the capacitance (during the anodic sweep) before leveling off to a relatively constant plateau. A similar type of curve was obtained during the cathodic sweep. The dashed lines in figure 7(a) represents the current required to charge the electrode capacitance. The small increasing currents above these plateaus are due, presumably, to small faradaic contributions. The geometric electrode capacitances, C_E, (farads/cm^2 of geometric area), using the anodic and cathodic currents at the middle of the potential sweep range (0.45 V), can be calculated as follows:

$$C_E = 0.5 \frac{(i_A + i_C)}{R} \tag{4}$$

where i_A and i_C are the anodic and cathodic current densities, respectively (mA/cm^2 of geometric area); and R is the sweep rate (mV/sec). A value of about 0.173 F/cm^2 was calculated for the initial cyclic sweep of electrode 5 prior to its being held at 0.6 V (fig. 7(a)). After the initial cycle sweep, electrode 5 was held at 0.6 V. The 0.6 V run was interrupted periodically for repeating the cyclic sweeps. As an illustration, the final cyclic voltammogram, obtained at the end of the 305 hr run, is shown in figure 7(b). This voltammogram was quite similar to the initial one shown in figure 7(a). The calculated geometric electrode capacitances are plotted in figure 23 against time held at 0.6 V. The capacitance values, which are related to the electrochemical surface areas of the electrode, decreased slightly during the first 20 hr after which they remained essentially constant at about 0.163 F/cm^2 for the rest of the run. This decrease in capacitance corresponds to a loss in active surface area of less than 5 percent during the first 20 hr. Therefore, it is assumed, that the change in the $Na_{0.75}Pt_3O_4$ electrode surface area was small and that most of the electrode structure remained relatively intact and in good contact with the current collector.

A measurement of a nonwetted sample of electrode 5 gave a value of about 1930 cm^2 of BET surface area per cm^2 of geometric surface. If this BET value is assumed for the

electrochemical active surface area (i.e., 100 percent utilization of electrocatalyst) and if the observed capacitance is assumed to be due to the double layer capacitance, the geometric capacitance value of 0.163 F/cm^2 yields a double layer capacitance of about 85 $\mu F/cm^2$ of true surface area for the $Na_{0.75}Pt_3O_4$ in electrode 5.

The outer surface of electrode 5 was grey-black after the 305 hr run at 0.6 V. However, x-ray diffraction analysis of the electrode after the run was in good agreement with the assumption of stability of $Na_{0.75}Pt_3O_4$ under reducing potentials. For example, the analysis yielded a value of 5.672 Å for the lattice constant. Equation 1 yields a composition of about $Na_{0.79}Pt_3O_4$ indicating that little or no change in the Na content occurred during the run within the estimated limits of error of about 0.005 for the lattice constant. Furthermore, decomposition of $Na_{0.75}Pt_3O_4$ during the run to form new phases was minimal since no new phases were observed in the x-ray diffraction within the limits of detection.

Electrode 5 was examined for stability in the presence of O_2. The sample of electrode 5 which had been used extensively for obtaining O_2 reduction and evolution current-potential data was analyzed by x-ray diffraction. The analysis indicated that no new phases were produced. In addition, the Na content in the electrode remained relatively unchanged from that of an unused electrode. For example, a value of 5.676 Å was obtained for the lattice constant in the used electrode. Equation 1 yields a composition of about $Na_{0.83}Pt_3O_4$ for the used sample.

Electrode 5 was also examined for stability in the presence of O_2 for longer periods under both oxidizing and reducing conditions. Electrode 5 was held anodically and then cathodically for a total of 281 hr at 24 °C (fig. 24). The increase in potential during the first 121 hr at an anodic current of 0.01 A was less than 0.1 mV/hr. Upon reversal to a cathodic current of -0.01 A, the potential decreased very rapidly to the cathodic steady-state potential but then remained essentially unchanged during the next 100 hr. Upon increasing the cathodic current to -0.1 A, the potential decreased rapidly to a new steady-state potential but then remained unchanged for the additional 60 hr. Therefore, relatively good stability is assumed for $Na_{0.75}Pt_3O_4$ for long periods of O_2 reduction and evolution. X-ray diffraction analysis of electrode 5 after the 281 hr test was in agreement with this assumption. For example, a value of 5.676 Å was obtained for the lattice constant indicating that the composition remained essentially unchanged.

For another series of tests under flowing O_2, electrode 5 was cycled at 0.01 and -0.01 A/cm^2 for alternate periods of 24 hr for a total of about 340 hr. The results are shown in figure 25. While the potentials appeared to increase slightly during each anodic 24 hr period, these potentials at the end of each anodic period were essentially the same value. For the cathodic 24 hr periods, the reverse appeared to be true. For example, the cathodic potentials remained essentially unchanged during each 24 hr period but decreased slightly after each previous anodic period. This decrease was still small, being less than 1 mV per cycle.

An electrode may be exposed to many oxidation and reduction potentials under O_2 during a moderate time period by continuous cycling. Electrode 5 was cycled continuously between 0.827 and 1.446 V at a scan rate of 1 mV/sec (fig. 21). The potential of 1.446 V was chosen to yield a relatively small anodic current of about 0.01 A/cm^2 which minimizes anodic polarization due to trapping of O_2 bubbles inside the electrode holder. Prior to the initiation of the cycling, the steady-state cathodic current at 0.827 V was determined to be -0.073 A. Changes in electrode activity during cycling may be determined by interrupting the cycling periodically and redetermining the steady-state cathodic currents at 0.827 V. These currents and iR

polarizations decreased slightly as the cycling proceeded. The slope for O_2 reduction, using the Tafel polarization plot in this region, was determined previously to be 0.04 V/decade. Each potential was then normalized by calculating the polarization potential that is necessary to restore the measured current to the initial current of -0.073 A. The normalized potentials (iR corrected) are plotted in figure 26 against the number of cycles. This decrease in potential was less than 10 μV/cycle suggesting relatively good $Na_{0.75}Pt_3O_4$ stability. X-ray diffraction analysis was in good agreement with this assumption. For example, analysis of electrode 5 after 1132 cycles (390 hr) indicated that the composition of the electrode remained relatively unchanged. A value of 5.677 Å was obtained for the lattice constant yielding a composition of about $Na_{0.84}Pt_3O_4$.

CONCLUDING REMARKS

1. The present study suggests that the PTFE-bonded $Na_XPt_3O_4$ gas porous diffusion electrode may be a viable electrocatalyst candidate for bifunctional O_2 reduction and evolution activity. The following results support this conclusion:

   a. The $Na_XPt_3O_4$ electrodes exhibited promising Tafel slopes of about 0.06 V/decade for both O_2 reduction and evolution at moderate current densities. "Apparent" activation energy values of about 5.6 and 9.5 Kcal/mol were calculated for O_2 reduction and evolution, respectively.

   b. O_2 reduction polarization for partially optimized electrode 5 was only somewhat larger than that reported for an IFC Au-10 percent Pt fuel cell O_2 electrode. O_2 evolution polarization for electrode 5 was similar to that reported for the active $NiCo_2O_4$ electrolysis electrode.

   c. For O_2 reduction, the 0.06 slope doubled to about 0.12 V/decade at larger current densities indicative of a change from activation to diffusion control for the gas porous diffusion electrodes examined. Further improvement in electrode performance may be possible if a more complete optimization of the electrode structure is accomplished.

   d. Voltage efficiencies of about 60 and 55 percent were estimated for O_2 reduction-oxidation processes at electrode 5 at 100 and 25 °C, respectively, for assumed anodic and cathodic current densities of -0.1 and 0.1 A/cm^2.

2. Stability testing at 24 °C suggests that $Na_XPt_3O_4$ electrodes are relatively stable at reducing and oxidizing potentials that might be encountered at the O_2 electrode in a fuel cell/electrolyzer system. The following results support this conclusion:

   a. The corrosion current for electrode 5 ($Na_{0.75}Pt_3O_4$) at 0.6 V under N_2 was less than 0.1 μA/mg of $Na_{0.75}Pt_3O_4$.

   b. While the electrode was being held at 0.6 V under N_2, the electrode capacitance of electrode 5 decreased less than 5 percent during the first 20 hr but then remained essentially constant for the remainder of the 305 hr test period.

c. The respective steady-state potentials of electrode 5 under O_2 were relatively constant at an anodic current of 0.01 A/cm^2 for 121 hr and at cathodic currents of -0.01 A/cm^2 for 100 hr and -0.1 A/cm^2 for 60 hr.

d. The respective steady-state potentials of electrode 5 under O_2 were relatively constant during cycling for 24 hr periods at alternate anodic and cathodic current densities of 0.01 and -0.01 A/cm^2 for a testing period of 340 hr.

e. The steady-state potentials of electrode 5 under O_2 were relatively constant at -0.073 A during continuous cycling between reducing and oxidizing potentials of 0.827 and 1.446 V, respectively, for a testing period of 1132 cycles (390 hr).

f. X-ray diffraction analyses indicated that secondary phases were not produced and that the Na content remained essentially unchanged during each of the stability testing runs.

3. Additional optimization of PTFE-bonded $Na_XPt_3O_4$ electrodes is warranted since the partially optimized $Na_{0.75}Pt_3O_4$ electrode 5 showed better bifunctional activity and stability than has been reported for any substance. Suggestions for further work are:

a. The effect of varying Na content (X = 0.7 to 1) in the $Na_XPt_3O_4$ powders upon activity and stability should be examined.

b. $Na_XPt_3O_4$ powders with surface areas greater than 20 m^2/g should be prepared. Improved morphology and particle size distribution of these powders is also desirable. For example, preparation from fine particle precursors may be very useful.

c. The effect of PTFE content should be examined in greater detail. For example, preliminary results for electrodes 1, 2, 3 and 4, which may have been too hydrophobic in character, suggested that maximum bifunctional O_2 activity may require an intermediate PTFE content. The effect of PTFE content upon electrode stability was not examined in the present study.

d. Catalyst and electrode processing should be critically investigated. Catalyst/PTFE processing and electrode fabrication conditions are important factors for optimizing the hydrophobic/hydrophilic character of the electrode and also for obtaining stable bonding of the electrocatalyst layer to the current collector. Furthermore, electrodes optimized for O_2 reduction may require different catalyst/PTFE processing conditions than required for O_2 evolution.

REFERENCE

1. Van Dine, L.; Gonzalez-Sanabria, O.; and Levy, A.: Regenerative Fuel Cell Study for Satellites in GEO Orbit. AIAA Paper 87–9200, Aug. 1987. (Also, NASA TM-89914).

2. Martin, R.E.: Advanced Technology Lightweight Fuel Cell Program. (FCR-1657, United Technologies Corp.) NASA CR–159807, 1980.

3. Fielder, W.L.; and Singer, J.: O_2 Reduction at the IFC Orbiter Fuel Cell O_2 Electrode. NASA TM–102580, 1990.

4. Trasatti, S.; and Lodi, G.: Oxygen and Chlorine Evolution at Conductive Metallic Oxide Anodes. Electrodes of Conductive Metallic Oxides, Part B, S. Trasatti, ed., Elsevier Scientific, 1981, pp. 521-626.

5. Fielder, W.L.; and Singer, J.: Oxygen Electrode Bifunctional Electrocatalyst $NiCo_2O_4$ Spinel. NASA TM–100947, 1988.

6. Swette, L.; and Kackley, N.: Rechargeable Alkaline Oxygen Electrode Development. Proceedings of the Symposium on Fuel Cells, R.E. White, and A.J. Appleby, eds., Electrochemical Society, 1989, pp. 216-233.

7. Shannon, R.D. et al.: Synthesis and Properties of Platinum Metal Oxides of the Type $M_XPt_3O_4$. Inorg. Chem., vol. 21, no. 9, 1982, pp. 3372-3382.

8. Schwartz, K.B.; et al.: Neutron Powder Diffraction Study of Two Sodium Oxides: $Na_{1.0}Pt_3O_4$ and $Na_{0.73}Pt_3O_4$. Acta Cryst. B, vol. 38, 1982, pp. 363-368.

9. Giner, J.; and Smith, S.: A Simple Method for Measuring the Polarization of Hydrophobic Gas Diffusion Electrodes. Electrochem. Technol., vol. 5, no. 1-2, 1967, pp. 59-61.

10. Tseung, A.C.C.; Jasem, S.; and Mahmood, M.N.: Oxygen Evolution on Porous Semiconducting Oxide Electrodes. Proceedings of the Symposium on Industrial Water Electrolysis, S. Srinivasan,; F.J. Salzano, and A.R. Landgrabe, eds., Electrochemical Society, 1978, pp. 161-168.

11. Giner, J. et al.: Methods for Characterizing the Structure and Electrochemical Behavior of Teflon-Bonded Pt Electrodes. J. Electrochem. Soc., vol. 116, no. 12, 1969, pp. 1692-1696.

12. Giner, J.; and Hunter, C.: The Mechanism of Operation of the Teflon-Bonded Gas Diffusion Electrode: A Mathematical Model. J. Electrochem. Soc., vol. 116, 1969, no. 8, pp. 1124-1130.

13. Gileadi, E.; Kirowa-Eisner, E.; and Penciner, J., eds.: Interfacial Electrochemistry: An Experimental Approach. Addison-Wesley, 1975, p. 74.

14. Power, G.P.; and Ritchie, I.M.: Metal Displacement Reactions. Modern Aspects of Electrochemistry, Vol. 11, B.E. Conway, and J.O'M. Bockris, eds., Plenum Press, 1975, pp. 199-250.

15. Bockris, J.O'M.; and Reddy, A.K.N.: Modern Electrochemistry. Vol. 1, Plenum Press, 1973, p. 547.

TABLE I.—PTFE-BONDED $Na_xPt_3O_4$ ELECTRODES

Electrode	$Na_{0.80}Pt_3O_4$ content, mg/cm^2	$Na_{0.75}Pt_3O_4$ content, mg/cm^2	PTFE content, percent of $Na_xPt_3O_4$
1	17	----	20
2	13.6	----	25
3	----	20	30
4	----	24.5	35
5	----	20	25

TABLE II.—O_2 REDUCTION AT $Na_XPt_3O_4$ ELECTRODES 1, 2, 3 AND 4

(a) 0.06 V/Decade region

Electrode	Intercept, V	Geometric exchange current density, A/cm^2 (normalized to 20 mg/cm^2)	Geometric current density range, A/cm^2
1	0.6014	$1.1x10^{-10}$	0.0001 to 0.0008
2	0.5386	$1.6x10^{-9}$	0.0001 to 0.001
3	0.4540	$2.7x10^{-8}$	0.0001 to 0.0012
4	0.4819	$7.6x10^{-9}$	0.0008 to 0.004

(b) 0.12 V/Decade region

1	0.7834	$3.5x10^{-7}$	0.0008 to 0.0016
2	0.7202	$1.5x10^{-6}$	0.001 to 0.0025
3	0.6286	$5.8x10^{-6}$	0.0012 to 0.005
4	0.6275	$4.8x10^{-6}$	0.004 to 0.010

TABLE III.—O_2 REDUCTION AT $Na_{0.75}Pt_3O_4$ ELECTRODE 5

(a) 0.04 V/Decade region

Temperature, °C	Intercept, V	Geometric exchange current density, A/cm^2	Geometric current density range, A/cm^2
24	0.3899	$1.8x10^{-10}$	0.002 to 0.025
33	0.3827	$2.7x10^{-10}$	0.002 to 0.025
50	0.3692	$5.9x10^{-10}$	0.001 to 0.025
71	0.3567	$1.2x10^{-9}$	0.0015 to 0.032
80	0.3536	$1.5x10^{-9}$	0.0015 to 0.040
93	0.3524	$1.6x10^{-9}$	0.001 to 0.050

(b) 0.06 V/Decade region

24	0.4218	$9.3x10^{-8}$	0.025 to 0.125
33	0.4149	$1.2x10^{-7}$	0.025 to 0.125
50	0.4038	$1.9x10^{-7}$	0.025 to 0.125
71	0.3877	$3.5x10^{-7}$	0.032 to 0.160
80	0.3810	$4.5x10^{-7}$	0.040 to 0.200
93	0.3774	$5.1x10^{-7}$	0.050 to 0.160

(c) 0.12 V/Decade region

24	0.4775	$1.1x10^{-4}$	0.125 to 0.320
33	0.4681	$1.3x10^{-4}$	0.125 to 0.320
50	0.4526	$1.7x10^{-4}$	0.125 to 0.320
71	0.4343	$2.4x10^{-4}$	0.160 to 0.400
80	0.4222	$3.0x10^{-4}$	0.200 to 0.400
93	0.4226	$3.0x10^{-4}$	0.160 to 0.400

TABLE IV.—O_2 EVOLUTION AT $Na_XPt_3O_4$ ELECTRODES 1, 2, 3 and 4

(a) 0.04 V/Decade region

Electrode	Intercept, V	Geometric exchange current density, A/cm^2 (normalized to 20 mg/cm^2)	Geometric exchange density range, A/cm^2
2	0.2692	$2.7x10^{-7}$	0.0002 to 0.003

(b) 0.06 V/Decade region

1	0.3290	$3.9x10^{-6}$	0.001 to 0.025
2	0.3192	$7.0x10^{-6}$	0.003 to 0.020
3	0.3010	$9.6x10^{-6}$	0.0001 to 0.0004
4	0.2703	$2.6x10^{-5}$	0.0006 to 0.0015

(c) 0.12 V/Decade region

1	0.4240	$3.5x10^{-4}$	0.025 to 0.125
2	0.4213	$4.5x10^{-4}$	0.020 to 1.160
3	0.5054	$6.1x10^{-5}$	0.0004 to 0.025
4	0.4394	$1.8x10^{-4}$	0.0015 to 0.005

TABLE V.—O_2 EVOLUTION AT $Na_{0.75}Pt_3O_4$

ELECTRODE 5 FOR THE 0.06 V/DECADE REGION

Temperature, °C	Intercept, V	Geometric exchange current density, A/cm^2	Geometric current density range, A/cm^2
24	0.3616	$9.4x10^{-7}$	0.001 to 0.013
37	0.3423	$2.0x10^{-6}$	0.001 to 0.025
49	0.3241	$4.0x10^{-6}$	0.001 to 0.040
63	0.3078	$7.4x10^{-6}$	0.001 to 0.025
76	0.2914	$1.4x10^{-5}$	0.001 to 0.020
88	0.2909	$1.4x10^{-5}$	0.001 to 0.032

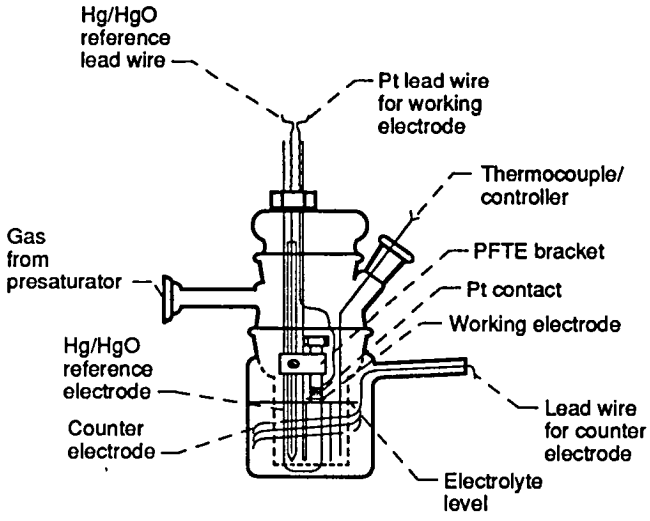

Figure 1.—Schematic of floating electrode half-cell apparatus.

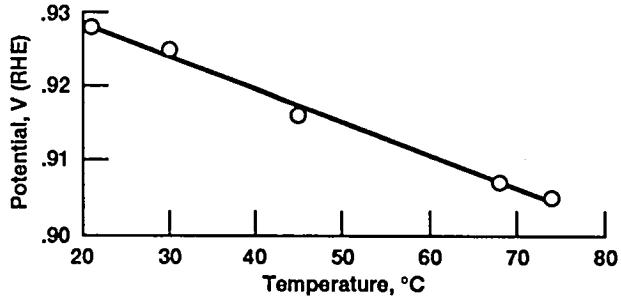

Figure 2.—Hg/HgO reference electrode potential with temperature (–0.45 mV/°C, 1 atm O_2, 30% KOH).

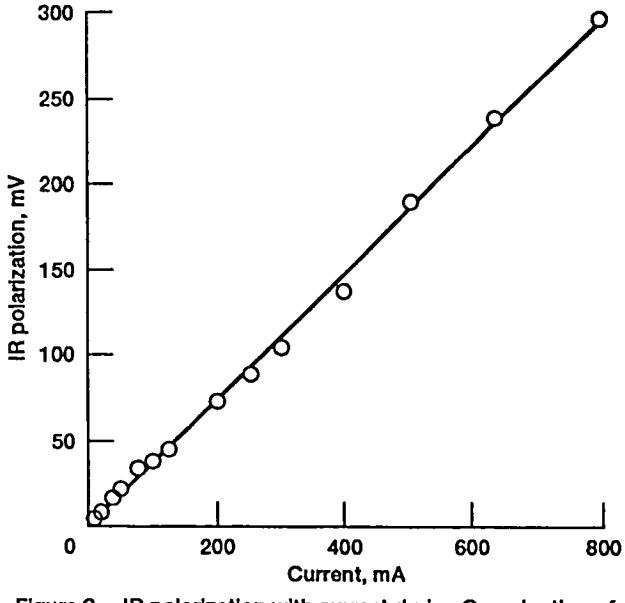

Figure 3.—IR polarization with current during O_2 reduction of electrode 5.

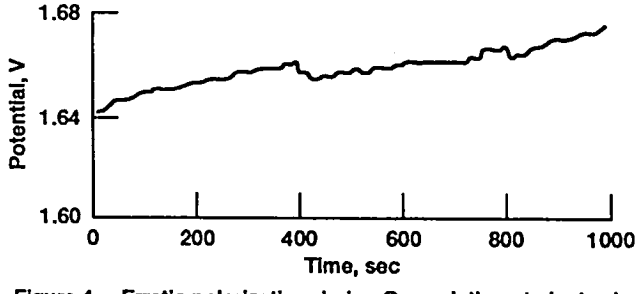

Figure 4.—Erratic polarization during O_2 evolution at electrode 5 (0.1 A/cm^2, 24 °C).

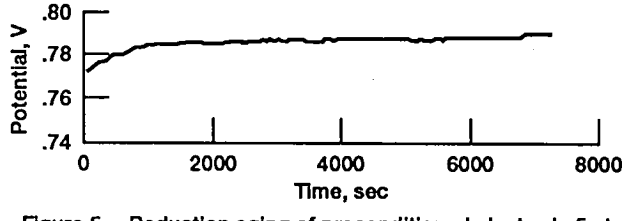

Figure 5.—Reduction aging of preconditioned electrode 5 at –0.01 A/cm^2 (24 °C).

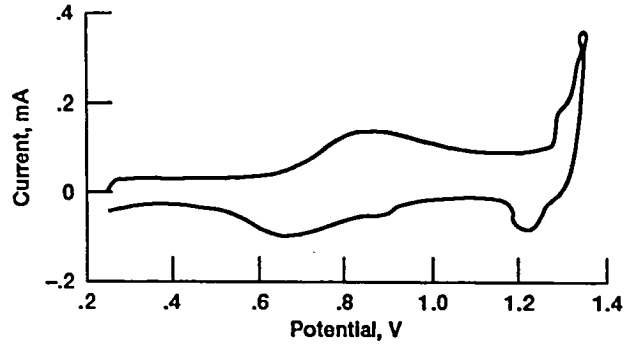

Figure 6.—Cyclic voltammogram of electrode 5 (0.3–1.4 V, 1 mV/sec, N_2, 24 °C, submerged).

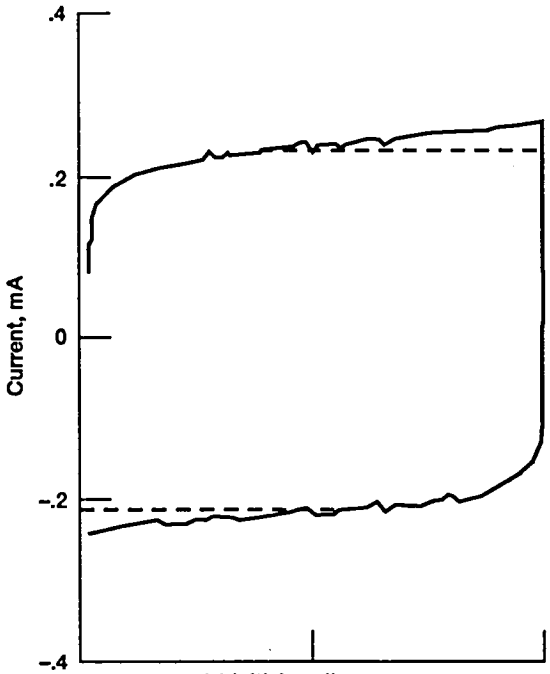

(a) Initial cyclic sweep.

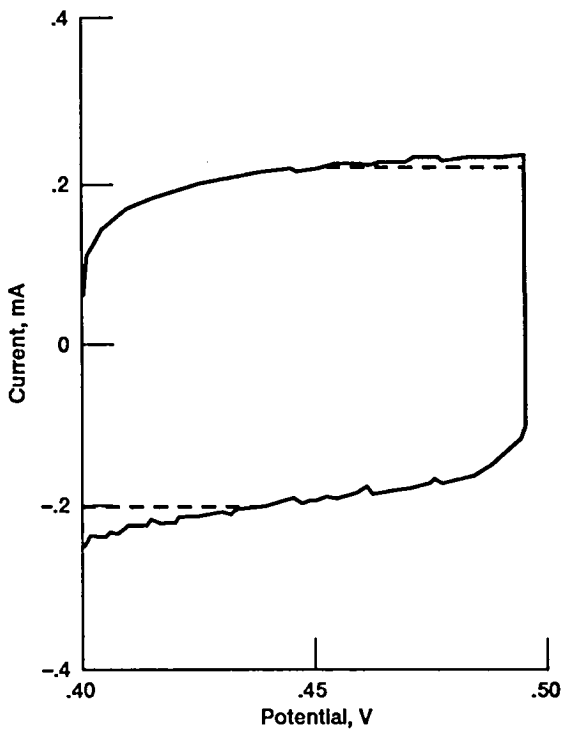

(b) Cyclic sweep after 305 hr at 0.6 V.

Figure 7.—Cyclic sweep of electrode 5 (0.4 to 0.5 V, 1 mV/sec, N_2, 24 °C, submerged).

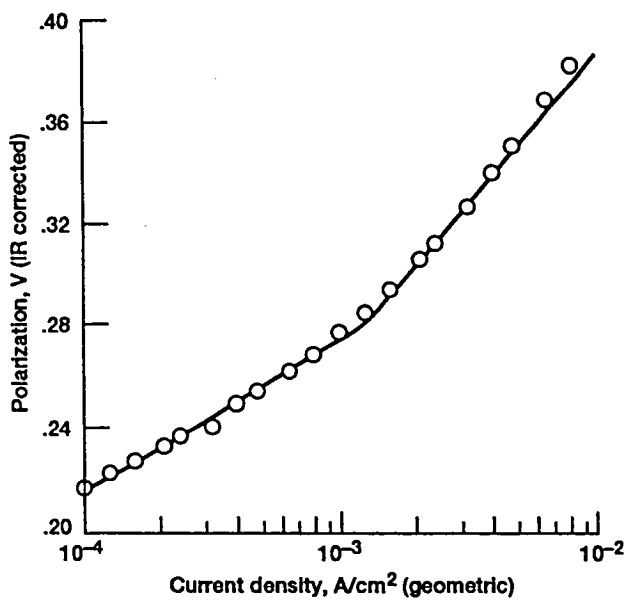

Figure 8.—Tafel plot for O_2 reduction at electrode 3 (80 °C, 1 atm O_2, 30% KOH).

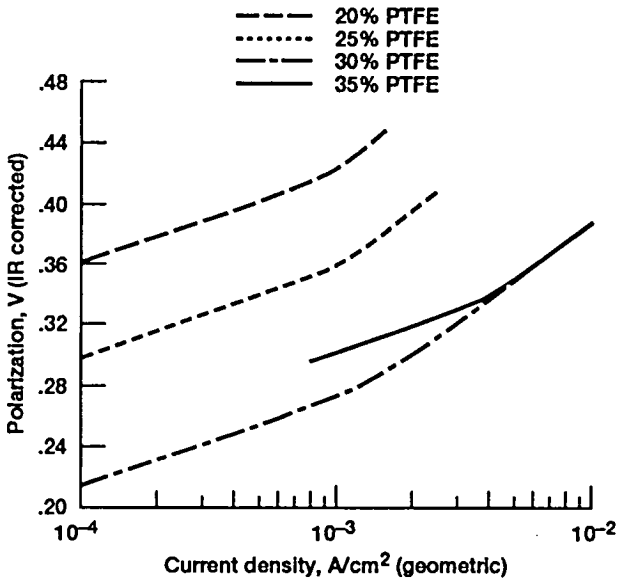

Figure 9.—Tafel plots for O_2 reduction at electrodes 1, 2, 3 and 4: normalized to 20 mg/cm^2 (80 °C, 1 atm O_2, 30% KOH).

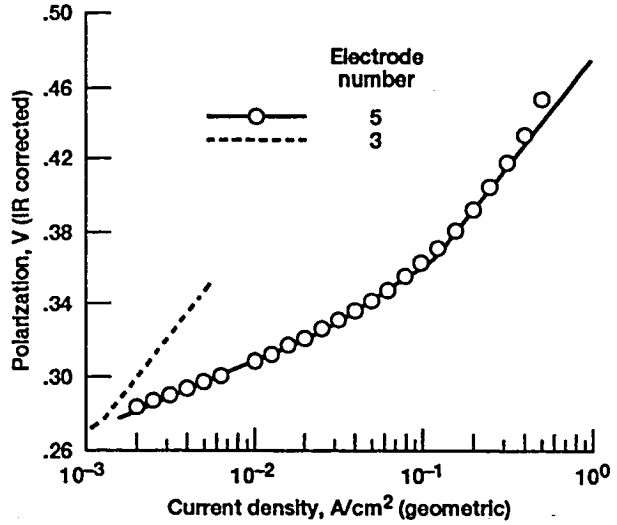

Figure 10.—Tafel plot for O_2 reduction at electrode 5 at 24 °C (electrode 3 at 80 °C, 1 atm O_2, 30% KOH).

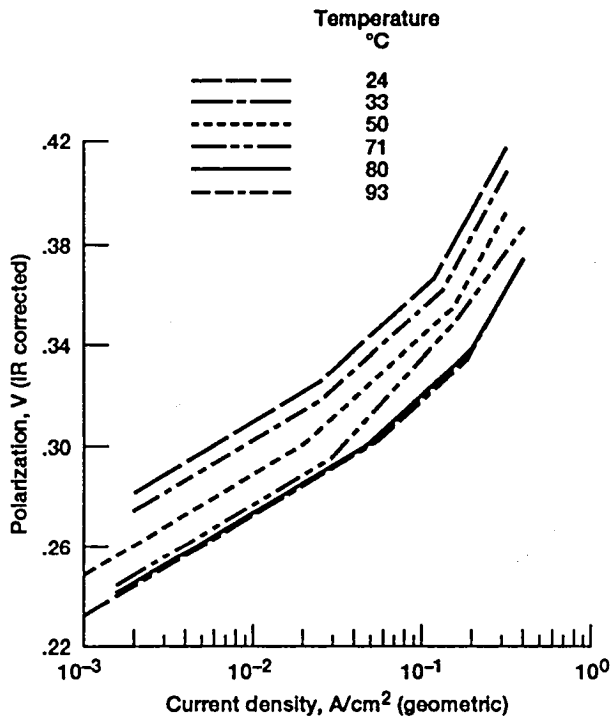

Figure 11.—Tafel plots for O_2 reduction at electrode 5 at various temperatures (1 atm O_2, 30% KOH).

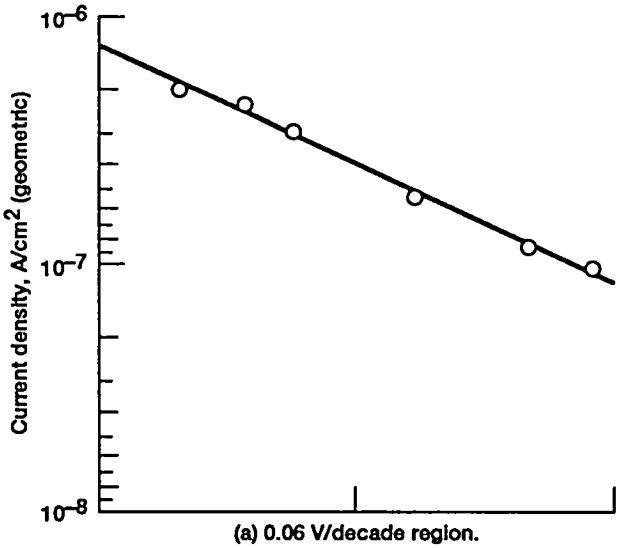

(a) 0.06 V/decade region.

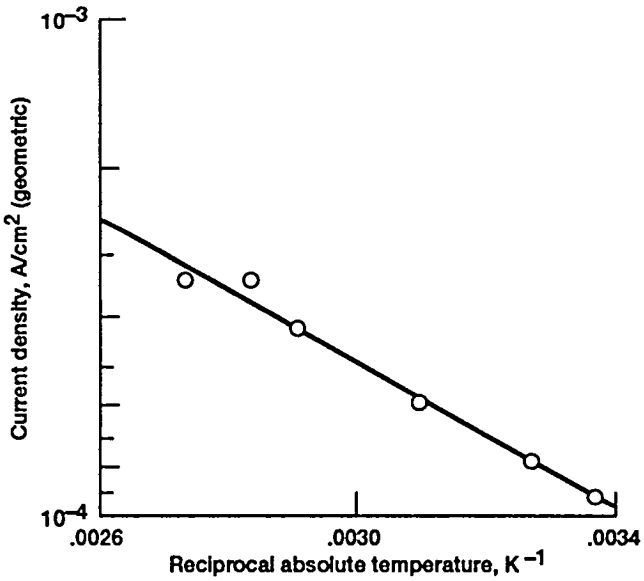

(b) 0.12 V/decade region.

Figure 12.—"Apparent" activation energy plot for O_2 reduction at electrode 5 (1 atm O_2, 30% KOH).

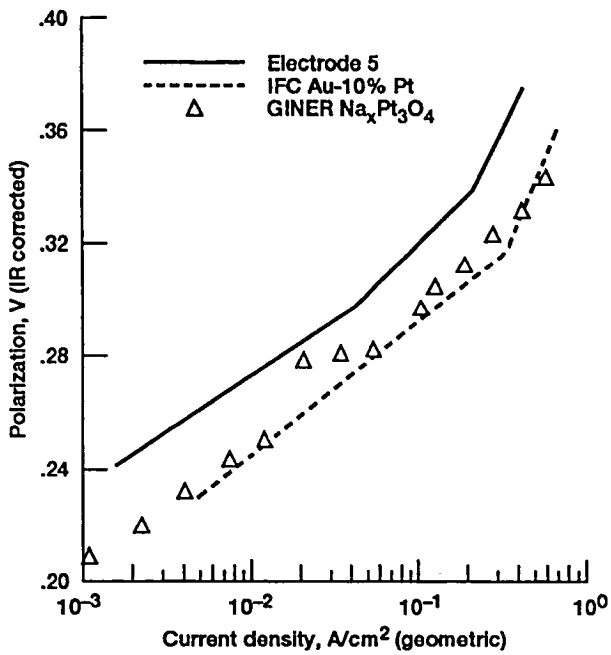

Figure 13.—Comparison of O_2 reduction polarization (80 °C, 1 atm O_2, 30% KOH).

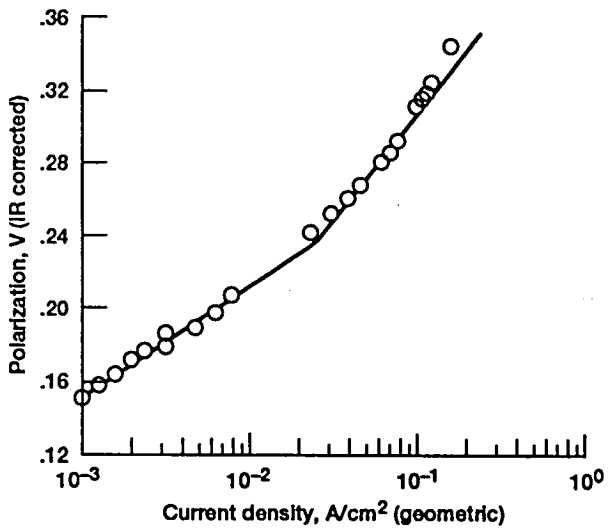

Figure 14.—Tafel plot for O_2 evolution at electrode 1 (80 °C, 1 atm O_2, 30% KOH).

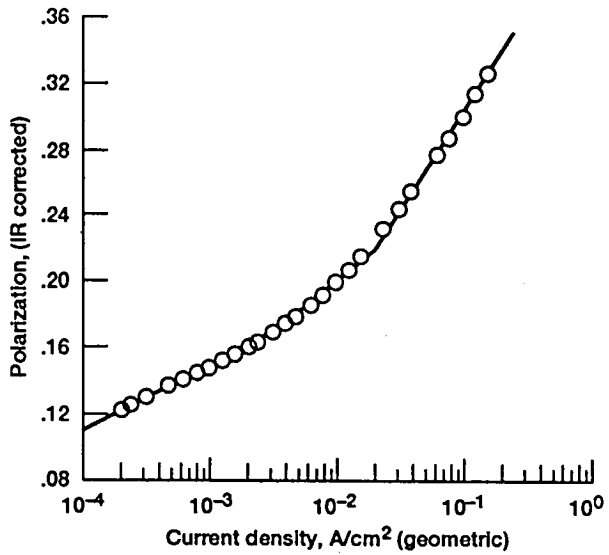

Figure 15.—Tafel plot for O_2 evolution at electrode 2 (80 °C, 1 atm O_2, 30% KOH).

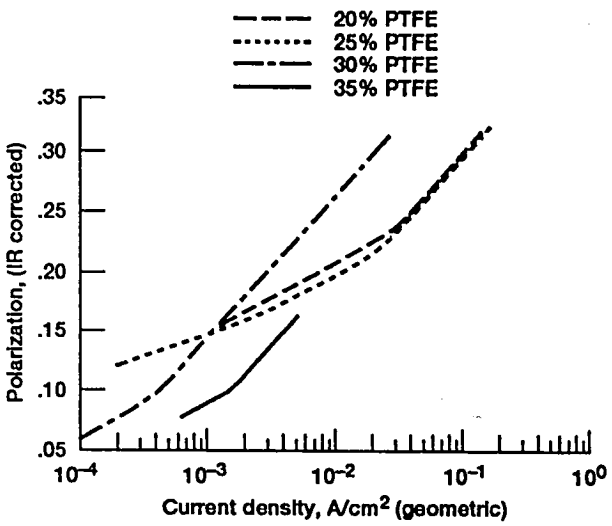

Figure 16.—Tafel plots for O_2 evolution at electrodes 1, 2, 3 and 4: normalized to 20 mg/cm^2 (80 °C, 1 atm O_2, 30% KOH).

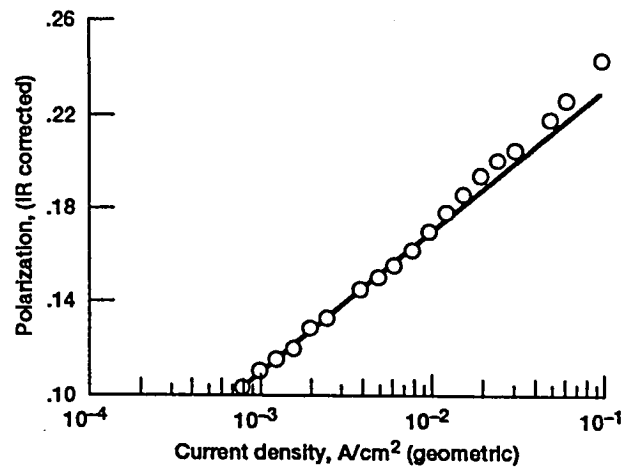

Figure 17.—Tafel plot for O_2 evolution at electrode 5 (88 °C, 1 atm O_2, 30% KOH).

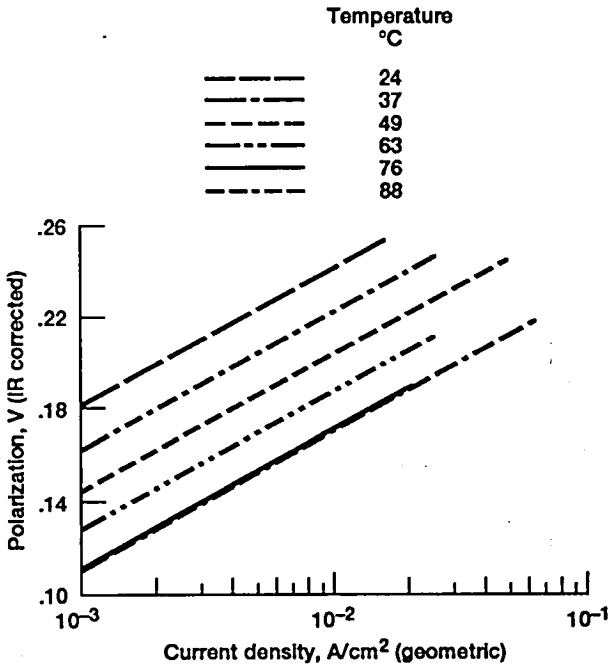

Figure 18.—Tafel plot for O_2 evolution at electrode 5 at various temperatures (1 atm O_2, 30% KOH).

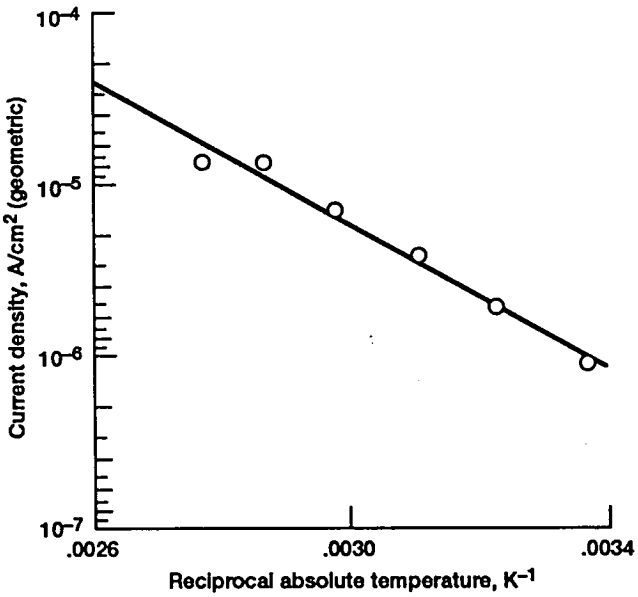

Figure 19.—"Apparent" activation energy plot for O_2 evolution at electrode 5 for the 0.06 V/decade region (1 atm O_2, 30% KOH).

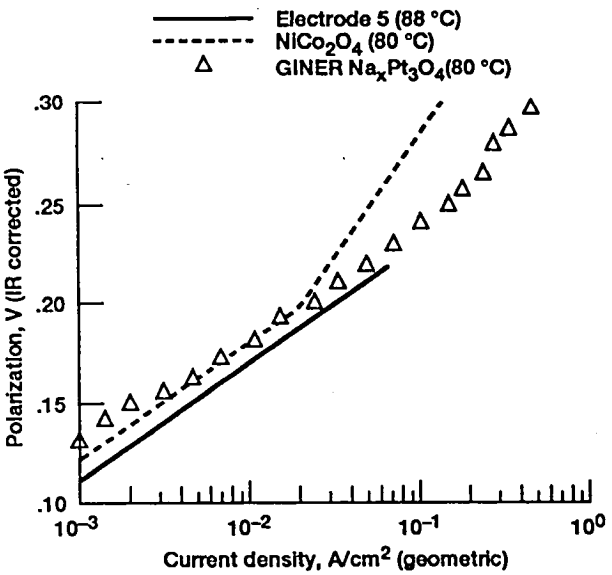

Figure 20.—Comparison of O_2 evolution polarization (80 °C, 1 atm O_2, 30% KOH).

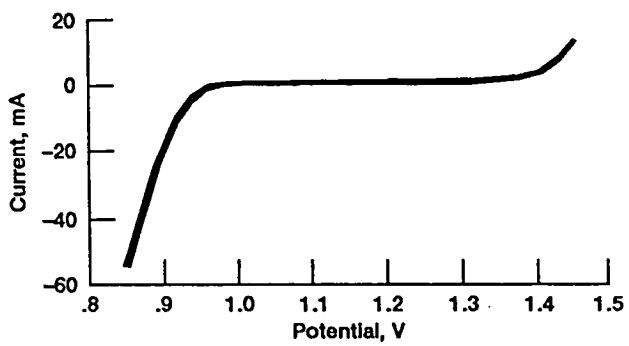

Figure 21.—Cyclic voltammogram of electrode 5 between 0.827 and 1.446 V at 1 mV/sec (24 °C, 1 atm O_2, 30% KOH).

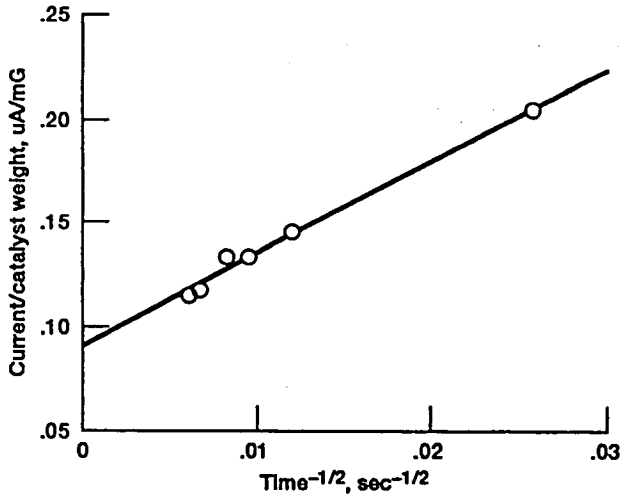

Figure 22.—Cathodic corrosion current for electrode 5 at 0.6 V (24 °C, 1 atm N_2, electrode submerged in 30% KOH).

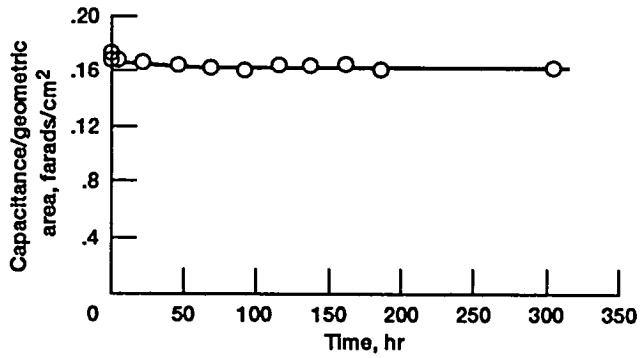

Figure 23.—Capacitance at 0.45 V with time for electrode for 5 held at 0.6 V (voltammogram between 0.4 and 0.5 V at 1 mV/sec, 24 °C, 1 atm N_2).

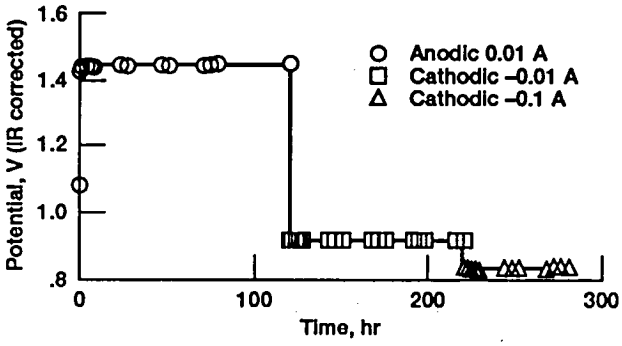

Figure 24.—Stability testing of electrode 5 held at anodic and cathodic potentials (24 °C, 1 atm O_2).

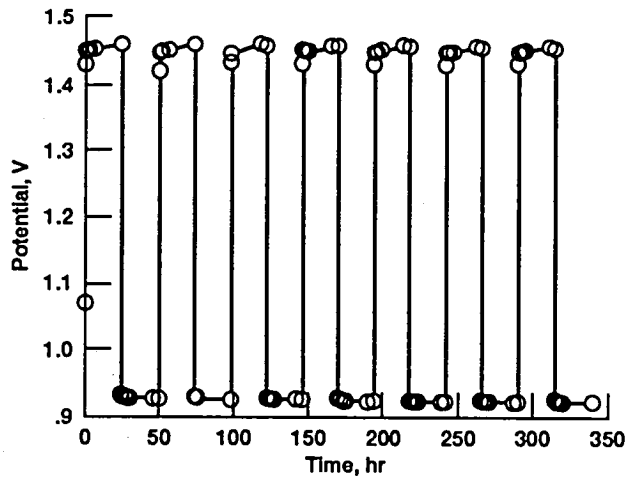

Figure 25.—Stability testing of electrode 5 during cycling at anodic 0.01 and cathodic –0.01 A/cm^2 (24 °C, 1 atm O_2).

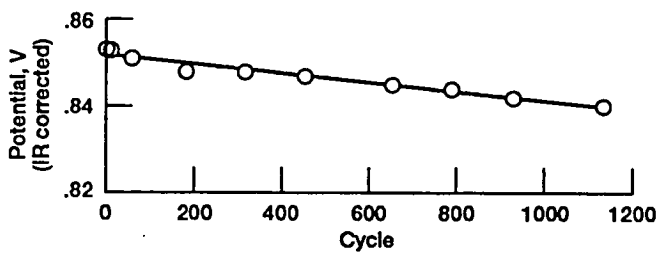

Figure 26.—Normalized potential of electrode 5 at –0.073 A with cycling between 0.827 and 1.446 V at 1 mV/sec (24 °C, 1 atm O_2).

REPORT DOCUMENTATION PAGE

Form Approved
OMB No. 0704-0188

1. AGENCY USE ONLY (*Leave blank*)	2. REPORT DATE	3. REPORT TYPE AND DATES COVERED
	December 1991	Technical Memorandum

4. TITLE AND SUBTITLE

A Study of $Na_xPt_3O_4$ as an O_2 Electrode Bifunctional Electrocatalyst

5. FUNDING NUMBERS

WU-506-42-21

6. AUTHOR(S)

William L. Fielder and Joseph Singer

7. PERFORMING ORGANIZATION NAME(S) AND ADDRESS(ES)

National Aeronautics and Space Administration
Lewis Research Center
Cleveland, Ohio 44135-3191

8. PERFORMING ORGANIZATION REPORT NUMBER

E-6664

9. SPONSORING/MONITORING AGENCY NAMES(S) AND ADDRESS(ES)

National Aeronautics and Space Administration
Washington, D.C. 20546-0001

10. SPONSORING/MONITORING AGENCY REPORT NUMBER

NASA TM-105311

11. SUPPLEMENTARY NOTES

Responsible person, William L. Fielder, (216) 433-5258.

12a. DISTRIBUTION/AVAILABILITY STATEMENT

Unclassified - Unlimited
Subject Category 20

12b. DISTRIBUTION CODE

13. ABSTRACT (*Maximum 200 words*)

The present study suggests that PTFE-bonded $Na_xPt_3O_4$ gas porous diffusion electrodes may be a viable candidate for bifunctional O_2 reduction and evolution activity. The electrodes exhibited Tafel slopes of about 0.06 V/decade for both O_2 reduction and evolution. For O_2 reduction, the 0.06 slope doubled to 0.12 V/decade at larger current densities. Preliminary stability testing at 24 °C suggested that the $Na_xPt_3O_4$ electrodes were relatively stable at reducing and oxidizing potentials typically encountered at the O_2 electrode in a regenerative fuel cell.

14. SUBJECT TERMS

Catalyst; Regenerative fuel cells

15. NUMBER OF PAGES

24

16. PRICE CODE

A03

17. SECURITY CLASSIFICATION OF REPORT	18. SECURITY CLASSIFICATION OF THIS PAGE	19. SECURITY CLASSIFICATION OF ABSTRACT	20. LIMITATION OF ABSTRACT
Unclassified	Unclassified	Unclassified	